Investigations of surface reactions during C_2F_6 plasma etching of SiO_2 with equipment and feature scale models

Da Zhang[a)]
Department of Materials Science and Engineering, University of Illinois, 1304 West Green Street, Urbana, Illinois 61801

Mark J. Kushner[b)]
Department of Electrical and Computer Engineering, University of Illinois, 1406 West Green Street, Urbana, Illinois 61801

(Received 18 September 2000; accepted 22 December 2000)

During fluorocarbon plasma etching of SiO_2, a polymer passivation layer is generally deposited on the surface of the wafer. The polymer layer regulates the etch by limiting the availability of activation energy and reactants, and providing the fuel for removal of oxygen. To investigate these processes, a surface reaction mechanism for fluorocarbon plasma etching of SiO_2 has been developed. The mechanism describes the polymerization process as resulting from neutral sticking, ion sputtering, F atom etching, and low-energy ion assisted deposition. The etch mechanism is a multistep passivation process which results in consumption of both the polymer and the wafer. The surface mechanism was incorporated into an equipment scale simulator to investigate the properties of SiO_2 etching in an inductively coupled C_2F_6 discharge, and predicts that the SiO_2 etch rate saturates at high substrate biases due to the depletion of passivation. Experimental results for SiO_2 etch rates and selectivity of SiO_2 over Si as a function of substrate bias were well reproduced. The blanket reaction mechanism was also employed in a feature scale simulator to investigate high aspect ratio (HAR) trench topography. Results from the feature scale model showed that strong sidewall passivation leads to tapered profiles in HAR SiO_2 etching. The incident ion energy and the ratio of the passivating neutral to ion fluxes largely determine the degree of the taper or bowing. Profile control can be obtained by regulating this ratio, with one such method being argon dilution.
 [DOI: 10.1116/1.1349728]

I. INTRODUCTION

Fluorocarbon plasma etching of SiO_2 is widely employed for the fabrication of multilayer ultralarge scale integrated circuits. It is well known that during fluorocarbon plasma processing, a CF_x polymer layer is deposited on the wafer surface thereby regulating the etch by limiting the delivery of activation energy and transport of reactants while at the same time providing one of the reactants.[1–5] The passivation layer also contributes to selectivity over Si. The CF_x polymer is deposited from C_xF_y neutrals or ions which have sufficient dangling bonds to insert into the polymer network. It is consumed by F atom etching and energetic ion sputtering.[6–8] Since the major roles of the polymer are to limit species diffusion through the layer and to dissipate ion bombarding energy, the etch rate generally scales inversely with the polymer thickness.[9–10] For example, in an investigation of SiO_2 etching in an inductively coupled plasma (ICP) sustained in C_2F_6, Oehrlein *et al.* observed an increasing etch rate with increasing substrate bias, which was attributed in part to the decreasing polymer thickness.[9] Similar dependencies of etch rate, polymer thickness, and substrate bias were also observed using CHF_3 plasmas.[10] Molecular dynamics simulations have been used to investigate CF_x etching of Si (Ref. 11) and fluorocarbon plasma etching of SiO_2 has been extensively experimentally investigated. There are, however, few theoretical descriptions which address the details of the polymerization kinetics and their relation to plasma conditions and etch properties.

In this work, a surface reaction mechanism for C_2F_6 plasma etching of SiO_2 is discussed. The mechanism was incorporated into a model for gas and surface processes in an ICP reactor and a parametric study of etch properties was performed. The reaction mechanism addresses polymer growth and SiO_2 etching resulting from a series of events including neutral passivation, ion assisted desorption, fluorination, and ion assisted chemical sputtering. The rates of these plasma-surface reactions generally depend on the thickness of the overlaying polymer. The mechanism was first applied to blanket etching in an integrated plasma equipment-surface kinetics model, the hybrid plasma equipment model-surface kinetics model (HPEM-SKM).[12] We found that the ion energy dependent sputtering yield of the polymer strongly regulates these processes due to their dependencies on the polymer thickness and the delivery of activation energy through the polymer. Ion energy is in turn controlled by the substrate bias. Low-energy ion activation of surface sites can assist in polymer formation and therefore suppress wafer etching. The etch selectivity of SiO_2 over Si is largely due to polymer etching by the oxygen in SiO_2

a)Present address: Motorola, Incorporated, 3501 Ed Bluestein Boulevard, Austin, Texas 78721; electronic mail: rgaabw@email.sps.mot.com
b)Author to whom correspondence should be addressed; electronic mail: mjk@uiuc.edu

which leads to thinner passivation on SiO_2 than on Si for the same process conditions. Good agreement for etch rates and selectivity between model and experimental results was achieved.

The reaction mechanism was also implemented into the Monte Carlo feature profile model (MCFPM)[13] to investigate the evolution of microtrenches etched in SiO_2. Similar dependencies of the etch rate on the substrate bias were obtained. Tapered profiles were produced for process conditions yielding strong sidewall passivation. Higher ion energies lead to less tapered profiles due to increasing polymer sputtering and more specular reflection. The degree of tapering also depends on the ratio of passivating neutral to ion fluxes, and so can be regulated by judicious choice of gas mixture, such as using argon dilution. Profiles transitioned from being tapered to straight to bowed as the passivating neutral to ion flux ratio decreased.

Descriptions of the HPEM-SKM and the MCFPM will be given in Sec. II, followed by a discussion of the surface reaction mechanism for SiO_2 etching by a C_2F_6 plasma in Sec. III. Results from the HPEM-SKM and the MCFPM simulations are presented in Secs. IV and V, respectively. Our concluding remarks are in Sec. VI.

II. DESCRIPTION OF THE MODELS

The integrated plasma equipment-surface kinetics model has been previously described and so will be only briefly discussed here.[12] The HPEM is a two-dimensional simulator with three main modules; the electromagnetic module (EMM), the electron energy transport module (EETM), and the fluid-chemical kinetics module (FKM). Electromagnetic fields and magnetostatic fields are calculated in the EMM. The EETM solves for electron impact source functions and transport coefficients based on these fields and electrostatic fields from the FKM. Results from the EETM are passed to the FKM, which computes the densities, momentum, and temperatures of plasma species, and the time varying electrostatic potential. The FKM outputs are then fed back to the EMM and EETM. This process iterates until results converge. The HPEM options used here are continuity, momentum, and energy for all neutral and ion species, and drift–diffusion transport for electrons. The EETM used the electron energy equation for bulk electron energy transport, and a Monte Carlo simulation for sheath accelerated secondary electrons.

Surface reactions in the HPEM are addressed by the SKM, an integrated module within the simulator framework. The SKM plays a dual role. First, it provides surface boundary conditions for the HPEM. The HPEM uses a flux in–flux out algorithm on surfaces. The fluxes incident onto surfaces in the HPEM are consumed with a specified probability and return fluxes of reactants from surfaces are produced with specified probabilities and branching ratios. The SKM provides these probabilities and branching ratios. Second, the SKM computes rates of material addition and removal on all surfaces in the reactor which, for the wafer, yields an etch rate. The SKM uses fluxes of reactants to surfaces supplied by the HPEM, and a user-defined surface reaction mechanism as input. The general form of a plasma–surface reaction in the mechanism is

$$A_g + B_s \rightarrow C_s + D_g + E_g, \tag{1}$$

where the subscript g denotes a gas species and the subscript s denotes a surface species. The rate for the ith reaction in the mechanism between species A and B and on material m, R_{im}, is

$$R_{im} = k_i \Phi^I_{Am} \theta_{Bm}, \tag{2}$$

where k_i is the reaction probability of the ith reaction, Φ^I_{Am} is the incident flux of plasma species A on material m, and θ_{Bm} is the fractional occupancy of the surface species B. The rates of evolution of the coverages of surface species are obtained by summing the rates of reactions generating or consuming the species, and are integrated in time using a third-order Runge–Kutta technique. The total fractional consumption for an incident species used in the HPEM is then the sum of fractional losses by all reactions removing the species. For an evolved gas species produced by, for example, an incident species A on a given material, the total fractional generation used in the HPEM is the summation of fractional generation by all reactions of reactant A which produces D on that material. The etch rate is obtained by summing over the rates of reactions converting surface species into volatile products.

The two-dimensional MCFPM was used to investigate profile evolution of SiO_2 trenches during C_2F_6 plasma etching. The MCFPM has been previously described so will be only briefly summarized here.[13,14] The MCFPM is an off-line module of the HPEM which resolves time dependent feature profiles resulting from plasma–surface interactions. Heavy particle transport in the HPEM is derived from fluid algorithms and so the angular and energy distributions of heavy particles required by the MCFPM are obtained from the plasma chemistry Monte Carlo simulation (PCMCS).[14] By using the plasma source functions and the electric fields available from the HPEM, the PCMCS calculates the energy distributions (ED) and angular distributions (AD) of neutral and charged heavy particles incident on specified surfaces. The plasma fluxes, EDs, and ADs are then supplied to the MCFPM. The MCFPM uses a rectilinear mesh to represent mask, wafer material, surface layers (such as polymer), and open areas occupied by plasma. Each cell in the mesh has a material identity. Pseudoparticles representing incident plasma species are launched into the system, following the EDs and ADs provided by the PCMCS. The pseudoparticles interact with the surface using essentially the same reaction mechanism as used in the equipment scale model, with the probability of each reaction being realized using Monte Carlo techniques. The consequences of these surface interactions include changing of the identity of the surface species mesh cell (for example, an adsorption event), addition or removal of surface species, and reflection and/or generation of plasma fluxes. The returning plasma species from the surface are tracked as new gas phase pseudoparticles.

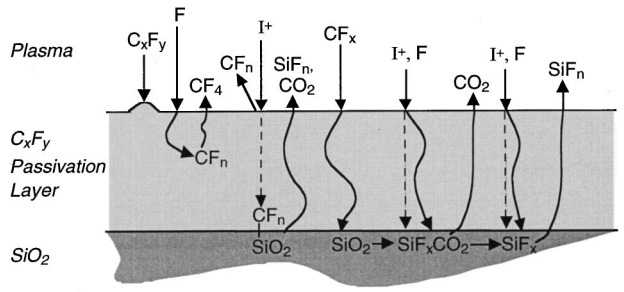

FIG. 1. Schematic of the surface reaction mechanism for SiO_2 etching by a fluorocarbon plasma. I^+ represents ion species. The dashed lines represent energy transfers through the polymer layer. The curved lines represent species diffusion through the polymer.

III. SURFACE REACTION MECHANISMS IN C_2F_6 PLASMA ETCHING OF SiO_2

The SiO_2 surface reaction mechanism is schematically shown in Fig. 1. The major steps in the mechanism are as follows. Polymer layers grow on the SiO_2 surface by C_xF_y deposition. Low-energy ion bombardment activates polymer surface sites which results in higher sticking coefficients for neutral radicals. Ion sputtering, F atom etching, and ion assisted polymer–wafer interactions consume the polymer. A steady state thickness of the polymer may be reached as a balance of its deposition and consumption. SiO_2 etching results from a polymer–wafer interaction which consumes both the SiO_2 wafer and the polymer. $CF_{x\leqslant 2}$ chemisorption on SiO_2 sites from either the polymer or directly from the plasma produces SiF_xCO_2 surface complexes which dissociate to SiF_x sites upon ion bombardment or F atom interaction. The SiF_x species are then removed by either ion chemical sputtering or F atom etching. The polymer passivation layer limits mass diffusion and dissipates energy, and so the rates of reactions involving energy transfer or species diffusion through the polymer depend on polymer thickness. The surface reactions encompassing this mechanism are listed in Table I. To investigate the etch selectivity of SiO_2 over Si, surface reactions appropriate for Si etching are also listed in Table I. The reaction probabilities in Table I are values for the base case which will be discussed in Sec. IV.

For surface processes involving ions (e.g., ion sputtering), the SKM use a general ion energy dependent reaction probability of the form[12]

$$p(E)=p_0\frac{E^x-E_{\text{th}}^x}{E_r^x-E_{\text{th}}^x}, \tag{3}$$

where E is the incident ion energy resulting from the acceleration in the plasma sheath, $p(E)$ is the reaction probability for an ion with energy E, E_{th} is the threshold energy of the process, E_r is a reference energy, and p_0 is the reaction probability at energy E_r. Experimental data indicate $x=0.5$ for our ranges of energy and this value was used here. The SKM uses time-averaged values for ion energies as appropriate for heavy ions.

The overlying polymer layers on SiO_2 influence the etch rate by limiting the fluxes of reactants to the wafer, dissipating ion bombarding energy, and by providing reactants for removal of oxygen from the film. SiO_2 and Si etch rates generally decrease with increasing polymer thickness due to this barrier to mass and energy transport.[5,9,10] The first step in describing the surface reaction mechanism is then to capture the kinetics of the polymer formation. The precursors for the polymer growth are generally believed to be C_mF_n radicals with a sufficient number of dangling bonds to insert into the polymeric network.[6–8,15] For example, Oehrlein *et al.* observed increasing passivation thickness with increasing CF_2 density in an ICP discharge sustained in CHF_3.[5] Booth *et al.* observed decreasing CF and CF_2 densities to the surface at low bias power in a CF_4 rf plasma, indicating surface consumption of these species whereas they observed CF_2 generation at high bias.[16] In our work, these polymerizing species are CF, CF_2, C_2F_3, and C_2F_4.

Measurements have shown that polymer layers can reach a steady state thickness during etching.[9,10] This implies that volumetric polymer consumption processes occur simultaneously to its deposition. One such process is F atom etching. F atoms terminate the dangling bonds of carbon in the polymer to form volatile products such as CF_4. As F atoms can diffuse into the polymer to react with the internal material, this process appears to be a bulk reaction. Another polymer consuming process is energetic ion sputtering. For example, Oehrlein *et al.* observed a decreasing polymer thickness with increasing substrate bias in inductively coupled plasmas.[10] In these systems, the substrate bias does not significantly change the magnitude of the reactant fluxes and only significantly changes the ion bombarding energy. As such, the decreasing passivation thickness with increasing bias should be attributed to the increasing rate of ion sputtering or ion activated process which consumes the polymer as opposed to a change in the composition of the flux. The sputtering process itself is likely more complicated in that it may involve chemical reactions as well as physical sputtering. For example, in addition to breaking polymer bonds, the energetic incident ions may dissociate to release F atoms which contribute to etching the film as well as inducing direct chemical reactions. In our reaction mechanism, however, we included only physical ion sputtering of the polymer with a reflection of the neutralized ion.

Another role ions may play in polymerization kinetics is activation of surface sites. Although sputtering likely dominates the consequences of ion bombardment on the polymerization kinetics when the ion energy is large (e.g., >100 eV), when the ion energy is low (≈ 10's eV), enhancement of polymer formation by ions has been observed. For example, Goto *et al.* investigated polymer growth on a grounded surface by a CF_2 beam coincident with an Ar microwave plasma.[17] The sheath potential was close to the floating plasma potential, which was estimated to be in the low 10's V, resulting in incident ion energies of a similar energy. They found that the polymer deposition rate was low when only the CF_2 beam was applied and that the deposition rates significantly increased with the addition of the Ar plasma. These observations were attributed to the low-energy ion ac-

TABLE I. Surface reaction mechanism. Species definitions: X_g, gas phase species; X_s, surface site; P, polymer layer component; and P^*, low-energy ion activated polymerization site.

Reaction[a,b]	Probability	Footnote
Polymer formation:	p_0	
$CF_{2g}+SiO_{2s}\rightarrow P+SiO_{2s}$	0.0033	c
$CF_{2g}+Si_s\rightarrow P+Si_s$	0.0033	c, i
$CF_{2g}+P\rightarrow P+P$	0.005	e, j
$CF_{2g}+P^*\rightarrow P+P$	0.08	e, j
$CF_g+SiO_{2s}\rightarrow P+SiO_{2s}$	0.0033	c
$CF_g+Si_s\rightarrow P+Si_s$	0.0033	c, i
$CF_g+P\rightarrow P+P$	0.005	e, j
$CF_g+P^*\rightarrow P+P$	0.08	e, j
$C_2F_{3g}+SiO_{2s}\rightarrow P+P+SiO_{2s}$	0.0033	c
$C_2F_{3g}+Si_s\rightarrow P+P+Si_s$	0.0033	c, i
$C_2F_{3g}+P\rightarrow P+P+P$	0.005	e, j
$C_2F_{3g}+P^*\rightarrow P+P+P$	0.08	e, j
$C_2F_{4g}+SiO_{2s}\rightarrow P+P+SiO_{2s}$	0.0033	c
$C_2F_{4g}+Si_s\rightarrow P+P+Si_s$	0.0033	c, i
$C_2F_{4g}+P\rightarrow P+P+P$	0.005	e, j
$C_2F_{4g}+P^*\rightarrow P+P+P$	0.08	e, j
Polymer consumption:	p_0	
$F_g+P\rightarrow CF_{4g}$	0.00057	h, j
$CF_3^+{}_g+P\rightarrow CF_{3g}+CF_{2g}$	$p_0=0.0225$	e, f, j
$CF_2^+{}_g+P\rightarrow CF_{2g}+CF_{2g}$	$p_0=0.0225$	e, f, j
$C_2F_4^+{}_g+P\rightarrow C_2F_{4g}+CF_{2g}$	$p_0=0.0225$	e, f, j
$C_2F_5^+{}_g+P\rightarrow C_2F_{5g}+CF_{2g}$	$p_0=0.0225$	e, f, j
$Ar^+{}_g+P\rightarrow Ar_g+CF_{2g}$	$p_0=0.0225$	e, f, j
Low-energy ion activation of polymerization site:	k_0	
$CF_3^+{}_g+P\rightarrow CF_{3g}+P^*$	0.011	e, g, j
$CF_2^+{}_g+P\rightarrow CF_{2g}+P^*$	0.011	e, g, j
$C_2F_4^+{}_g+P\rightarrow C_2F_{4g}+P^*$	0.011	e, g, j
$C_2F_5^+{}_g+P\rightarrow C_2F_{5g}+P^*$	0.011	e, g, j
$Ar^+{}_g+P\rightarrow Ar_g+P^*$	0.011	e, g, j
Ion assisted polymer–SiO_2 interaction:	p_0	
$CF_3^+{}_g+P+SiO_{2s}\rightarrow SiF_{2g}+CO_{2g}+CF_{3g}+SiO_{2s}$	0.023	d, f
$CF_2^+{}_g+P+SiO_{2s}\rightarrow SiF_{2g}+CO_{2g}+CF_{2g}+SiO_{2s}$	0.023	d, f
$C_2F_4^+{}_g+P+SiO_{2s}\rightarrow SiF_{2g}+CO_{2g}+C_2F_{4g}+SiO_{2s}$	0.023	d, f
$C_2F_5^+{}_g+P+SiO_{2s}\rightarrow SiF_{2g}+CO_{2g}+C_2F_{5g}+SiO_{2s}$	0.023	d, f
$Ar^+{}_g+P+SiO_{2s}\rightarrow SiF_{2g}+CO_{2g}+Ar_g+SiO_{2s}$	0.023	d, f
Neutral passivation:	p_0	
$CF_{2g}+SiO_{2s}\rightarrow SiF_2CO_{2s}$	0.0085	d
$CF_g+SiO_{2s}\rightarrow SiFCO_{2s}$	0.0085	d, j
Fluorination:	p_0	
$F_g+Si_s\rightarrow SiF_s$	0.008	d, j
$F_g+SiF_s\rightarrow SiF_{2s}$	0.008	d, j
$F_g+SiF_{2s}\rightarrow SiF_{3s}$	0.0085	d, j
$F_g+SiF_{3s}\rightarrow SiF_{4g}+SiO_{2s}$	0.0085	d, j
$F_g+SiF_{3s}\rightarrow SiF_{4g}+Si_s$	0.0085	d, j
$F_g+SiF_2CO_{2s}\rightarrow SiF_{3s}+CO_{2g}$	0.0085	d
$F_g+SiFCO_{2s}\rightarrow SiF_{2s}+CO_{2g}$	0.0085	d
Ion activated dissociation:	p_0	
$CF_3^+{}_g+SiF_2CO_{2s}\rightarrow SiF_{2s}+CF_{3g}+CO_{2g}$	0.1	d, f
$CF_3^+{}_g+SiFCO_{2s}\rightarrow SiF_s+CF_{3g}+CO_{2g}$	0.1	d, f
$CF_2^+{}_g+SiF_2CO_{2s}\rightarrow SiF_{2s}+CF_{2g}+CO_{2g}$	0.1	d, f
$CF_2^+{}_g+SiFCO_{2s}\rightarrow SiF_s+CF_{2g}+CO_{2g}$	0.1	d, f
$C_2F_4^+{}_g+SiF_2CO_{2s}\rightarrow SiF_{2s}+C_2F_{4g}+CO_{2g}$	0.1	d, f
$C_2F_4^+{}_g+SiFCO_{2s}\rightarrow SiF_s+C_2F_{4g}+CO_{2g}$	0.1	d, f
$C_2F_5^+{}_g+SiF_2CO_{2s}\rightarrow SiF_{2s}+C_2F_{5g}+CO_{2g}$	0.1	d, f
$C_2F_5^+{}_g+SiFCO_{2s}\rightarrow SiF_s+C_2F_{5g}+CO_{2g}$	0.1	d, f
$Ar^+{}_g+SiF_2CO_{2s}\rightarrow SiF_{2s}+Ar_g+CO_{2g}$	0.1	d, f
$Ar^+{}_g+SiFCO_{2s}\rightarrow SiF_s+Ar_g+CO_{2g}$	0.1	d, f
Ion chemical sputtering:	p_0	
$CF_3^+{}_g+SiF_s\rightarrow SiF_{2g}+CF_{2g}+SiO_{2s}$	0.11	d, f
$CF_3^+{}_g+SiF_{2s}\rightarrow SiF_{2g}+CF_{3g}+SiO_{2s}$	0.11	d, f
$CF_3^+{}_g+SiF_{3s}\rightarrow SiF_{4g}+CF_{2g}+SiO_{2s}$	0.11	d, f
$CF_2^+{}_g+SiF_s\rightarrow SiF_{2g}+CF_g+SiO_{2s}$	0.11	d, f
$CF_2^+{}_g+SiF_{2s}\rightarrow SiF_{2g}+CF_{2g}+SiO_{2s}$	0.11	d,f
$CF_2^+{}_g+SiF_{3s}\rightarrow SiF_{4g}+CF_g+SiO_{2s}$	0.11	d, f
$C_2F_4^+{}_g+SiF_s\rightarrow SiF_{2g}+C_2F_{3g}+SiO_{2s}$	0.11	d, f
$C_2F_4^+{}_g+SiF_{2s}\rightarrow SiF_{2g}+C_2F_{4g}+SiO_{2s}$	0.11	d, f
$C_2F_4^+{}_g+SiF_{3s}\rightarrow SiF_{4g}+C_2F_{3g}+SiO_{2s}$	0.11	d, f
$C_2F_5^+{}_g+SiF_s\rightarrow SiF_{2g}+C_2F_{4g}+SiO_{2s}$	0.11	d, f
$C_2F_5^+{}_g+SiF_{2s}\rightarrow SiF_{2g}+C_2F_{5g}+SiO_{2s}$	0.11	d, f
$C_2F_5^+{}_g+SiF_{3s}\rightarrow SiF_{4g}+C_2F_{4g}+SiO_{2s}$	0.11	d, f
$Ar^+{}_g+SiF_s\rightarrow SiF_g+Ar_g+SiO_{2s}$	0.11	d, f
$Ar^+{}_g+SiF_{2s}\rightarrow SiF_{2g}+Ar_g+SiO_{2s}$	0.11	d, f
$Ar^+{}_g+SiF_{3s}\rightarrow SiF_{3g}+Ar_g+SiO_{2s}$	0.11	d, f

[a]Unless otherwise specified, all ions neutralize on all surfaces, returning as their neutral counterparts.
[b]All gas phase species have units of flux ($cm^{-2}\,s^{-1}$). All surface species have units of fractional coverage.
[c]Process limited to surface sites not covered by polymer.
[d]Process rate depends on the polymer coverage. See Eq. (5).
[e]Process limited to the top layer of the polymer.
[f]See Eq. (3). $E_r=70$ eV, $E_{th}=3$ eV.
[g]See Eq. (4). $E_c=65$ eV unless otherwise specified.
[h]Bulk process.
[i]Equivalent process in Si etching.
[j]Process also valid for Si etching.

tivation of polymeric surface sites for neutral radical sticking. With this mechanism, the low CF_2 self-sticking probability suggested by Sawin *et al.* in the absence of ion bombardment,[18] and the high effective CF_2 sticking rate at low power rf discharge observed by Booth *et al.*,[16] can be rationalized. The observations of Oehrlein *et al.* of increasing polymer thickness with decreasing bias made in this low energy regime, are also consistent with an increase in the efficiency of ion activation for polymerization with decreasing ion energy. We modeled this ion activation process as having a probability, k, of

$$k=k_0\times\max\left(0,\ 1-\frac{E_i}{E_c}\right), \tag{4}$$

where E_i is the incident ion energy, E_c is the maximum

energy of the process, and k_0 is the probability at zero incident ion energy. After being activated, a surface site is then more likely to chemisorb polymerizing neutrals.

Another polymer consuming process occurs at the polymer–wafer interface. Experiments have shown that for the same process conditions, passivation is thinner on SiO_2 than on Si.[9] After the passivation thickness exceeds one monolayer, the kinetics of polymer growth should be the same regardless of the underlying wafer material if the kinetics depends only on the incident neutral and ion fluxes. The observation that the polymer thickness depends on the wafer material implies that reactions at the polymer–wafer interface are capable of consuming the polymer. In the case of SiO_2 substrates, oxygen atoms in the film can react with the carbon atoms in the polymer, etching the wafer, consuming the passivation, and releasing volatile products such as CO_2.[19] The polymer-etching ability of oxygen atoms is well known, as oxygen plasmas are often used to strip photoresist and an analogous process is observed during etching.[19,20] These polymer–wafer interactions do, however, require activation energy. This energy is delivered by ion bombardment through the overlying polymer layer. During the transfer of the bombarding ion energy through the overlying layers, some portion of the energy is dissipated in the polymer by bond breaking and heating, with only a fraction reaching the surface. Consequently, the efficiency of the energy transfer and activation of these processes decreases with increasing polymer thickness, resulting in the probabilities of polymer–wafer reactions depending on the polymer thickness. Following this logic, we used the following expression for the dependence of processes at the surface which require ion activation energy,

$$c = c_0 \lambda, \quad \lambda = \frac{1}{1 + \alpha \cdot [P] + \gamma \cdot [P]^2}, \tag{5}$$

where c is the reaction probability, $[P]$ is the number of overlying polymer monolayers, c_0 is the reaction probability when no polymer is present, λ is the power transfer efficiency, and α and γ are constants. In this work, we used $\alpha = 0.6$ and $\gamma = 0.1$.

Polymer–surface interactions also contribute to wafer etching. The carbon atoms in the polymer in the form of CF_x in contact with SiO_2, coincident with ion bombardment through the polymer layer, abstract oxygen atoms from the oxide. This process evolves volatile CO containing products and leaves the target Si atoms in the oxide partially passivated by F atoms. F atoms which diffuse through the polymer further passivate the $Si–F_x$ sites, eventually forming volatile SiF_n products. In this regard, the first layer of the polymer passivation acts as a precursor for etching.

A second pathway for passivation of SiO_2 sites is through direct $CF_{x\leq 2}$ neutral chemisorption to form SiF_xCO_2 intermediate complexes. These complexes dissociate to SiF_x surface sites and CO_2 gas upon ion bombardment or F atom passivation. As in Si etching, F atoms then saturate the dangling bonds of the remaining $Si–F_x$ sites, resulting in volatile products. Lastly, due to the comparatively thin polymer passivation on SiO_2, incident energetic ions can penetrate through the polymer and directly chemically sputter surface species. All such processes have lower probabilities in Si etching due to the thicker polymer layer, thereby contributing to selectivity of SiO_2 over Si in fluorocarbon etching.

On nonwafer surfaces, we employed a simpler reaction mechanism where CF and CF_2 stick with a probability of 0.01. CF_3 recombines to form C_2F_6 with a probability of 0.01 and F recombines to form F_2 with a probability of 0.005.

We note that the SiO_2–polymer interface is likely not a well-defined boundary. Molecular dynamics simulations have shown considerable mixing of CF_x and Si in the topmost layers of Si following energetic CF_3^+ bombardment.[21] This mixing likely also occurs during SiO_2 etching, but is not directly addressed here. We also note that negative ions do not appear in the surface reaction mechanism while they are part of the gas phase reaction mechanism. For the processing conditions of interest, the negative ion flux to the substrate is negligible due to the always negative substrate bias and large, positive plasma potential. In pulsed plasma systems, significant fluxes of negative ions can reach the substrate. Applying this model to pulsed systems may require amendments to the reaction mechanism to account for the consequences of negative ions.

In the discussion that follows, we use the number of polymer monolayers to represent the polymer thickness. We assumed each monolayer contains 10^{15} cm^{-2} carbon atoms. For a polymer composition and density which mimic $(C_2F_4)_n$, each monolayer is ≈ 6 Å thick.

IV. ETCHING OF SiO_2 IN A C_2F_6 PLASMA

SiO_2 etching in an inductively coupled discharge sustained in C_2F_6 was investigated with the integrated plasma equipment and surface kinetics model. To enable comparison with experiments and to facilitate calibration of the mechanism, the reactor geometry, and the process conditions follow those of Oehrlein *et al.*[9] The cylindrical reactor is schematically shown in Fig. 2. Inductive power is supplied through a three-turn coil 16 cm in diameter. The coil sits on a 2 cm thick quartz window which is 23 cm in diameter. The wafer is on a substrate located 7 cm below the quartz window and upon which a rf bias is applied. The source gas is supplied from a ring nozzle located under the quartz window. The gas inlet flow rate is 40 sccm and the gas pressure is maintained at 6 mTorr by throttling the pump rate. The coil source current is at 13.56 MHz, delivering 1400 W of inductive power. The frequency of the rf bias is 3.4 MHz, and the base case amplitude of the bias is 100 V. The bias voltage is used to control the ion bombarding energy while it has a small influence on other plasma conditions. The gas phase reaction mechanism in the model is similar to that reported in Ref. 11 with the addition of reactions to produce and consume CF, CF_2^+, and dissociation (both neutral and dissociative attachment) of F_2.

Typical plasma properties for the base case are shown in

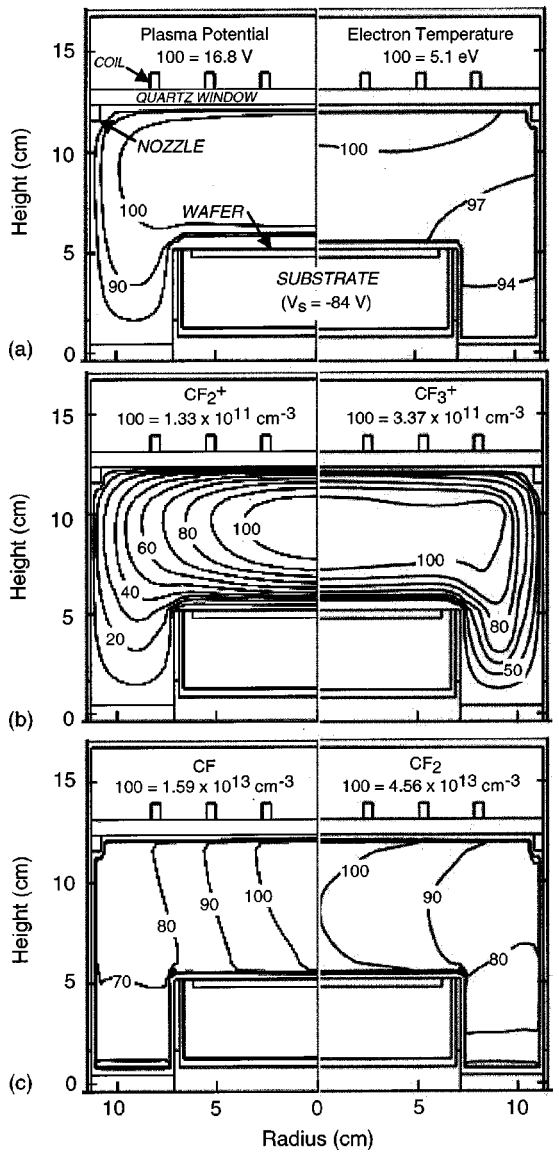

FIG. 2. Plasma properties for the base case (C_2F_6, 1400 W ICP power, 6 mTorr, 40 sccm, 100 V bias). (a) Plasma potential and electron temperature. (b) CF_2^+ and CF_3^+ densities. (c) CF and CF_2 densities. The labels on the contour lines are a percentage of the maximum value shown at the top of each figure.

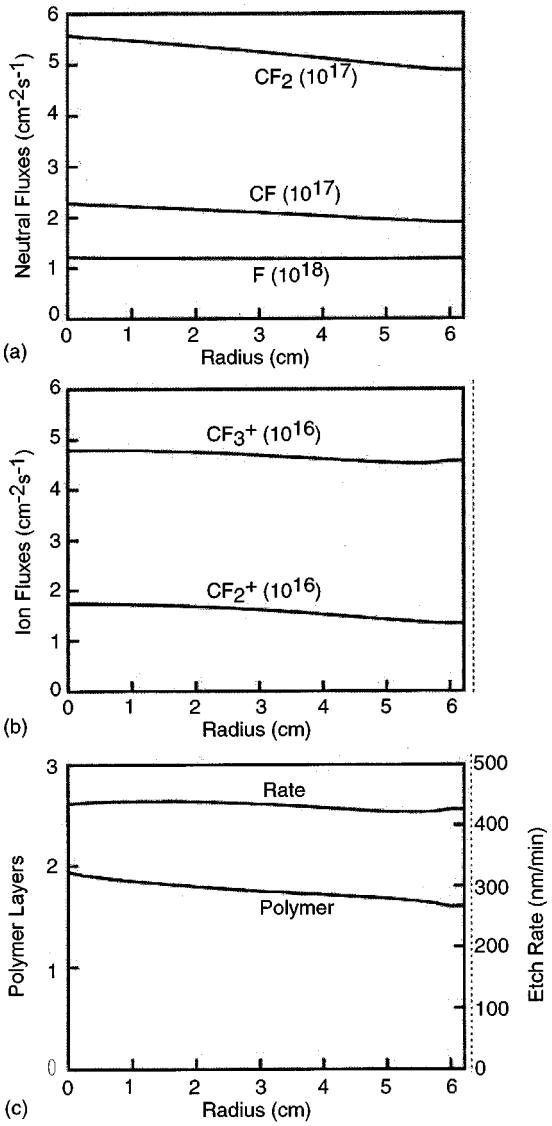

FIG. 3. Plasma and process properties at the wafer as a function of radius for the base case. (a) Fluxes of CF_2, CF, and F. (b) Fluxes of CF_3^+ and CF_2^+. (c) Polymer layers and etch rates. A decreasing polymer thickness with radius is compensated for by a decreasing ion flux to yield a uniform etch rate.

Fig. 2. The electron temperature (T_e) peaks near the inductive source where the azimuthal electric field and the power deposition are maximum, as shown in Fig. 2(a). T_e changes little within the plasma chamber. At this low pressure, the electron density is high (2.7×10^{11} cm^{-3}) and the electron–neutral collision frequency is small, producing a large plasma conductivity. This also leads to a quite uniform plasma potential in the process chamber, as shown in Fig. 2(a). To balance the currents in the asymmetric reactor, a negative voltage, the self-bias voltage, is generated, which in this case is -84 V. Although the time averaged plasma potential peaks at only 16.8 V, the time averaged sheath potential above the wafer is 98 V. The CF_3^+ and CF_2^+ ion densities are shown in Fig. 2(b) and contribute to a peak positive ion density of 4.7×10^{11} cm^{-3}. As diffusive transport dominates at low pressure, both densities peak near the center of the reactor. Since one of the major sources for CF_3^+ is the electron impact ionization of the feedstock C_2F_6 gas, whose density is largest near the ring nozzle, its peak area expands to larger radii. CF_2^+, which is dominantly produced by ionization of dissociation products of C_2F_6, has a density which is more diffusion dominated. The two ion densities are of the same order, though CF_3^+ is the more abundant species. CF and CF_2 radical densities are shown in Fig. 2(c). The high input power produces ≈95% dissociation of the C_2F_6 as well as heating of the gas to a peak value of ≈500 K above the 350 K walls. As a result neutral products having highest densities are F, CF_2, and CF, which do not have C–C bonds. Both the CF and CF_2 densities are fairly uniform. Fluxes of C_2F_3, C_2F_4, $C_2F_4^+$, and $C_2F_5^+$ are smaller than those of the

TABLE II. Reactant fluxes to the center of the wafer. Process conditions: C_2F_6, 6 mTorr, 1400 W ICP power, 40 sccm gas flow rate, 100 V bias.

Species	Flux ($cm^{-2}\,s^{-1}$)
CF_2	5.58×10^{17}
CF	2.28×10^{17}
C_2F_3	9.50×10^{14}
C_2F_4	1.02×10^{15}
F	1.21×10^{18}
CF_3^+	4.78×10^{16}
CF_2^+	1.74×10^{16}
$C_2F_4^+$	2.28×10^{14}
$C_2F_5^+$	3.45×10^{13}

C-monomer species due to the highly dissociating environment.

Radical and ion fluxes to the wafer surface for the base case are shown in Fig. 3 and are listed in Table II. As a consequence of the uniform gas phase distributions, the fluxes are also fairly uniform, in general having a small maximum on axis. The fluxes of CF_2 and CF, the major precursors for polymer deposition, decrease a bit more in the radial direction than do the ion and F atom fluxes, which consume the polymer. This leads to a small radial decrease of the polymer thickness, as shown in Fig. 3(c). Although the decreasing polymer thickness as a function of radius would normally enhance the rate of SiO_2 etching, the decrease in ion flux with increasing radius, which activates the etch, partially compensates. As a result, the SiO_2 etch rate is more uniform than that of the polymer thickness, as shown in Fig. 3(c).

The influence of ion energy on SiO_2 etching was investigated by varying the rf bias. Increasing substrate bias does not appreciably change the plasma potential, however it does increase the magnitude of the self-bias voltage on the substrate, which increases the time averaged sheath potential above the wafer. For example, the magnitude of the self-bias voltage (V_s), and the sheath potential drop above the wafer (V_d), as a function of the substrate bias, are shown in Fig. 4. (These values are actually negative. However, to avoid confusion, we will be referring to the magnitude in our discussion.) Both V_s and V_d increase linearly with substrate bias. A similar linear relationship between the self-bias voltage and

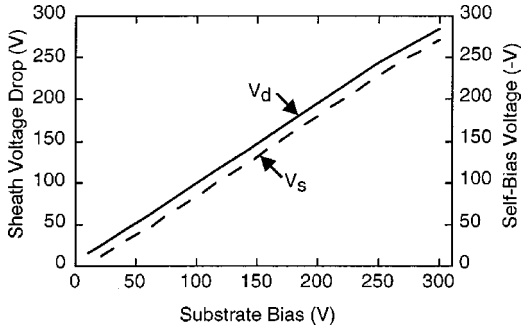

FIG. 4. Sheath voltage drop and self-bias voltage at the wafer surface as a function of substrate bias. The self-bias voltages are negative.

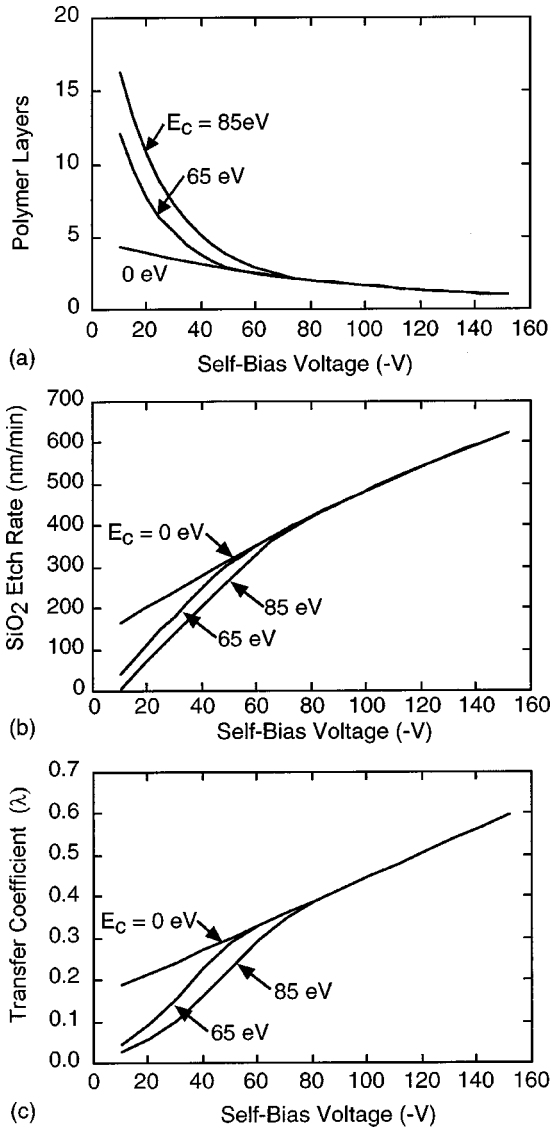

FIG. 5. Surface process properties as a function of the self-bias voltage for different E_c, the threshold for ion activated sticking. (a) Polymer thickness. (b) Etch rate. (c) Power transfer coefficient λ. Increasing E_c produces thicker polymer layers and lower etch rates.

substrate bias power was obtained by Oehrlein *et al.* in a CHF_3 discharge in the same reactor and using the same process conditions.[22] There was little variation in the model in the magnitude of the ion flux to the substrate with bias voltage (<3%). This trend also agrees with the observations of Oehrlein *et al.* that the ion current density measured with a Langmuir probe changes little with rf bias power.[22]

The polymer thickness as a function of the self-bias voltage for different E_c, the maximum energy for ion activation of polymerizing sites, is shown in Fig. 5. When no such ion activation process is used ($E_c=0$), decreasing polymer thickness with increasing V_s was observed, which is largely due to the increasing ion sputtering of the polymer and ion activated etching. At $V_s=30$ V, the proportions of polymer consumption by F atom etching, ion sputtering, and ion activated etching are 1:0.3:0.1. At $V_s=150$ V, these propor-

tions are 1:3.6:1.3. The decreasing polymer thickness favors transfer of energy and etchant through the passivation to the wafer surface. As a result, the etch rate increases as shown in Fig. 5(b). The general trends obtained with $E_c=0$ agree with most experiments.[9,10] However, the sharp increase in passivation thickness and the decrease in etch rate (or onset of deposition) with decreasing V_s in the low bias region, which are usually observed experimentally,[9,10] are not captured with $E_c=0$. This implies that there may be some additional low-energy ion assisted polymerization process. By including such a process into the mechanism, using an energy dependent activation efficiency described in Eq. (4), the polymer thickness was found to be sensitive to the maximum ion activation energy, E_c. For example, when $E_c=65$ eV, a sharp increase of polymer thickness with decreasing V_s was obtained at low biases, as shown in Fig. 5(a). The increasing thickness results in wafer etching processes involving energy transfer or species diffusion through the polymer being less efficient, as shown by the energy transfer coefficient (λ) in Fig. 5(c). This leads to a decrease in etch rate at $E_c=65$ eV as compared with $E_c=0$. The differences in polymer thickness and etch rate between $E_c=65$ eV and $E_c=0$ increases with decreasing bias, because the ion activation efficiency increases with decreasing ion energy and the transfer efficiency decreases. A further increase in E_c to 85 eV results in an additional increase of polymer thickness and decrease in etch rate in the low bias region.

The delivery of activation energy through polymer layers, and its effect on etch rates, has recently been investigated by Tatsumi *et al.* for a high plasma density, dual frequency reactive-ion-etching system operating in $C_4F_8/Ar/O_2$ mixtures.[23] By operating in thin-to-thick polymer regimes while keeping ion fluxes constant, they were able to estimate the effective energy delivered to the polymer–SiO_2 interface as a function of polymer thickness. They found that for polymer thicknesses of $P=1-8$ ($\approx 0.5-5$ nm), the energy transfer coefficient varied from $\lambda=0.93$ to 0.48 for a fixed bias of 1450 V. This decrease in energy transfer to the surface was reflected in a decrease in surface reactivity and etch rate.

To validate the model and to calibrate parameters in the reaction mechanism, computed results were compared to experiments[9] for SiO_2 and Si etch rates as a function of self-bias voltage, as shown in Fig. 6(a). For these results, $E_c=65$ eV. The process conditions in the model are the same as in the experiment and there is generally good agreement. Etch rates asymptote to zero at finite bias, increasing with a steep slope to about 60 V. Rates increase with a shallower slope at higher voltages. The etch selectivity of SiO_2 over Si is in part due to differences in the thickness of the passivation as shown in Fig. 6(b). Ion assisted polymer–wafer interactions occur for SiO_2 etching, which, for lack of oxygen atoms to react with the polymer, are absent for Si etching. This leads to thinner polymer passivation on SiO_2 than on Si for the same process conditions, and more efficient transfer of energy and reactants to the wafer in SiO_2 etching, also shown in Fig. 6(b). The transfer coefficient λ increases more rapidly with bias for SiO_2 than for Si due to

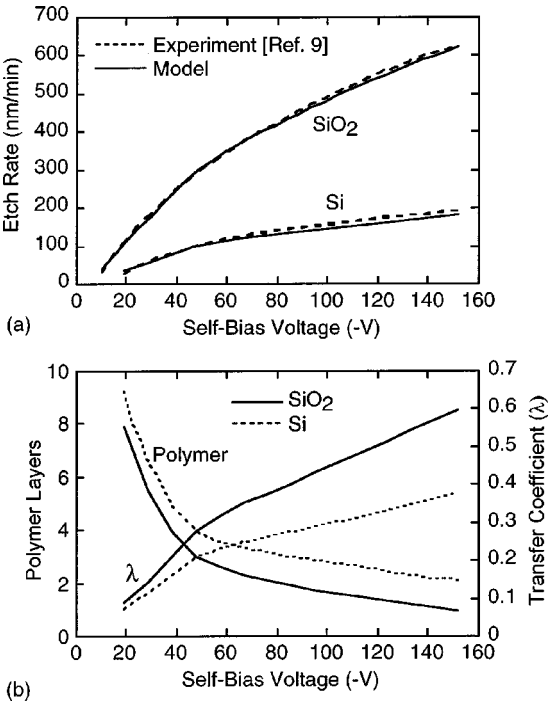

FIG. 6. SiO_2 and Si etch properties as a function of self-bias voltage. (a) Simulated and experimental results (Ref. 9) for SiO_2 and Si etch rates. The model results are for $E_c=65$ eV. (b) Model results for polymer thickness and transfer coefficient (λ) in SiO_2 and Si etching.

the thinner polymer. The thinner passivation on SiO_2 also makes it possible for energetic ions to penetrate through the polymer and chemically sputter the wafer,[9,24] contributing to additional selectivity over Si.

To investigate etching at high ion energies, we extended our study to higher biases than were covered in the experiments. Other process parameters follow those for the base case. The SiO_2 etch rate and the polymer thickness as a function of the self-bias voltage are shown in Fig. 7(a) in solid lines. The passivating neutral to ion flux ratio is $\beta=\Phi_n/\Phi_{\text{ion}}=12$ and the average ion energy is approximately the same as the bias voltage. In the high ion energy range (>150 eV), the etch rate tends to saturate. This is due to the depletion of the polymer passivation. Recall that etching of SiO_2 requires CF_x for volatilization of both the Si and O. The CF_x can be supplied either directly by neutral adsorption or by the first layer of passivation. When the ion energy exceeds 150 eV, the passivation drops below 1 monolayer. For ion energies greater than 250 eV, the passivation covers only a small fraction (~ 0.3) of surface sites. As a result, the etch process is limited by the availability of neutral passivation which serves as a precursor for SiO_2 etching.

If this analysis is correct, the etch rate in the passivation-starved regime ($\geqslant 150-200$ V) should decrease if β is decreased, while in the low energy regime where the polymer thickness is already above one layer, the etch rate should increase if β is decreased. The passivating neutral flux was artificially decreased by 30% with respect to that obtained in the base case simulation, yielding $\beta=8.4$. The results are shown in Fig. 7(a) as dashed lines. Through the entire range

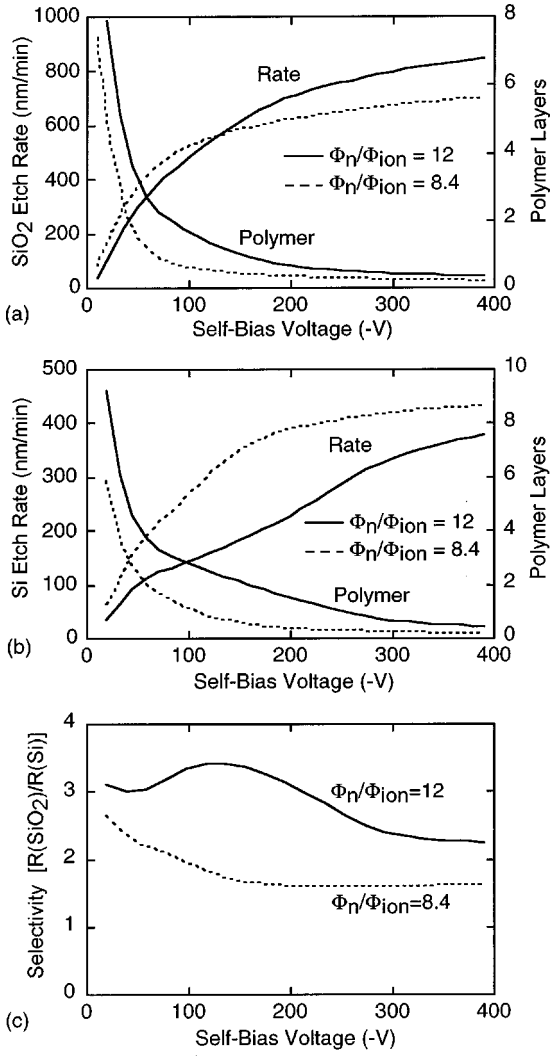

FIG. 7. SiO_2 and Si etch properties as a function of ion energy for different passivation neutral to ion flux ratios (Φ_n/Φ_{ion}). (a) Polymer thickness and etch rate for SiO_2 etching. (b) Polymer thickness and etch rate for Si etching. (c) Etch selectivity of SiO_2 over Si. SiO_2 etch rates saturate at high bias and low Φ_n/Φ_{ion} due to starvation of passivation.

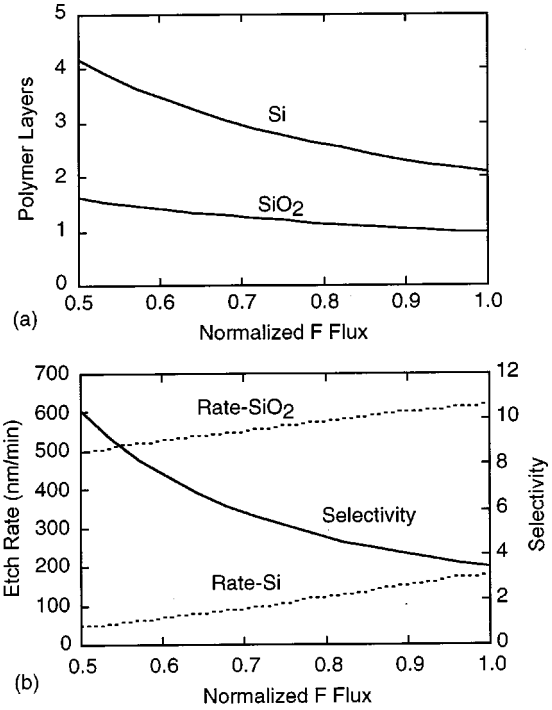

FIG. 8. SiO_2 and Si etch properties as a function of F atom flux. (a) Polymer thickness. (b) Etch rates and selectivity. The F atom fluxes were normalized to the value obtained at 170 V bias. Large F atom fluxes produce thinner polymer layers and low selectivity. Decreasing the F atom flux reduces the Si etch rate more rapidly than that for SiO_2, thereby improving selectivity.

of biases the polymer thickness decreases with decreasing β due to the smaller amount of precursor. In the low energy regime where the polymer is thick and its major influence is limiting the transfer of energy and species, the decrease of polymer thickness leads to an increase in the etch rate. In the high energy regime, the polymer is thin and its influence on energy or species transfer is less significant. The thin passivation does, however, limit the availability of CF_x precursors. Therefore reducing β actually leads to a drop in the etch rate. These trends are not observed for Si, as shown in Fig. 7(b). Here the polymer thickness decreases with decreasing β as for SiO_2. However, the etch rate always increases with decreasing β and decreasing polymer thickness because the passivation layer serves only as a barrier to transport and not as a precursor for Si etching.

The etch selectivity, defined as the etch rate of SiO_2 over Si, for the two values of β as a function of self-bias voltage is shown in Fig. 7(c). For these process conditions, decreasing the passivating neutral flux leads to a larger decrease of passivation on Si than on SiO_2 and a larger increase in etch rate. As a result the etch selectivity decreases with decreasing β. The high ICP power produces a large density of F atoms, which etch the polymer layers in both SiO_2 and Si processing. Consequently, for the same process conditions the difference in polymer thickness on SiO_2 and Si is not large. As a result the etch selectivity obtained is not large. For example, at 170 V bias and $\beta=12$, the etch selectivity is 3.4.

One approach for improving the etch selectivity is to reduce the F atom density so that polymer thicknesses are larger. This goal can be met by choosing a different chemistry or by equipment design. For instance, adding hot Si surfaces in addition to the wafer to the plasma chamber can consume F atoms by forming SiF_x compounds, a strategy used in commercial plasma etching tools. To demonstrate this strategy, the F atom flux was artificially changed based on the results obtained at 170 V bias. The process properties as a function of F atom flux (normalized to the value at 170 V) are shown in Fig. 8. For both SiO_2 and Si etching, the polymer thickness increases with decreasing F atom flux due to the lower rate of polymer etching. As a consequence, the etch rates for Si and SiO_2 increase with decreasing F atom flux. However, due to the dominance of F atom etching in polymer consumption during Si etching, the polymer thickness changes more rapidly on Si than on SiO_2. As a result, the relative decrease in etch rate with decreasing F atom flux is larger for Si than for SiO_2. This produces an increase in

the etch selectivity with decreasing F atom flux, as shown in Fig. 8(b).

Due to the lack of fundamental data, the reaction probabilities used in the model were more or less determined by calibration with experiments from Oehrlein *et al.*[9] Some of these reaction probabilities may change with reactor conditions. For example, neutral sticking probabilities on chamber walls change with surface temperature which in turn affect etch characteristics.[5] Given these uncertainties in choosing the probabilities, it is valuable to investigate the sensitivity of the model to the variation of these parameters. We first varied the sticking coefficient, σ, for passivating neutrals to polymerize on an unactivated polymer surface site. The base case value is $\sigma = 0.005$, and σ was parametrized from 0.003 to 0.007. (The probability for sticking on an ion-activated site is 0.08.) The radial distributions of polymer thickness and etch rate for different σ are shown in Fig. 9 for a substrate bias of 100 V. The polymer thickness logically increases with increasing σ because of the increase in the deposition source and the increase in polymer thickness produces a decrease in the etch rate. Since there is little ion assisted polymerization for this bias ($E_c < V_s$), neutral polymerization occurs at only unactivated sites. As a result, the increase in polymer thickness scales within σ. Note, however, that the polymer thickness increases more rapidly than σ. This results from the fact that as the polymer thickens λ, the energy transfer coefficient decreases, thereby decreasing the rate of polymer consumption on the wafer. The polymer thickness and etch rate as a function of the self-bias voltage for different values of σ are shown in Figs. 9(c) and 9(d), respectively. The absolute increase in polymer thickness is proportional to the increase in σ and, indirectly, to the decrease in λ resulting from the increase in thickness. However in the low bias region, there is additional passivation on ion activated sites and so the relative change in polymer thickness with varying σ is smaller than that in the high bias region. For $\sigma = 0.007$, the polymer is more than one monolayer throughout the bias range. Consequently, the SiO_2 etch rate increases with V_s with a slope that changes little from low bias to high bias, as shown in Fig. 9(d). With smaller σ, the polymer thickness drops below one monolayer at high biases. This leads to a saturation of the etch rate due to lack of CF_x precursor.

As ion sputtering is a major consumer of the polymer, its probability was also parametrized. The polymer thickness as a function of p_0 for different substrate biases is shown in Fig. 10(a) where for the base case $p_0 = 0.025$. For all biases the polymer thickness decreases with increasing p_0. When the bias is low (<40 V), the small ion sputtering rate and the ion assisted polymerization combine to make the passivation thick and polymer consumption is dominated by F atom etching. The resulting smaller λ produces lower etch rates and lower rates of polymer consumption. When the bias voltage is high (>100 V), the polymer is thin and to a large degree its consumption is determined by ion sputtering. As a result, increasing p_0 leads to a larger relative decrease in the polymer thickness than at low biases. Consequently the etch

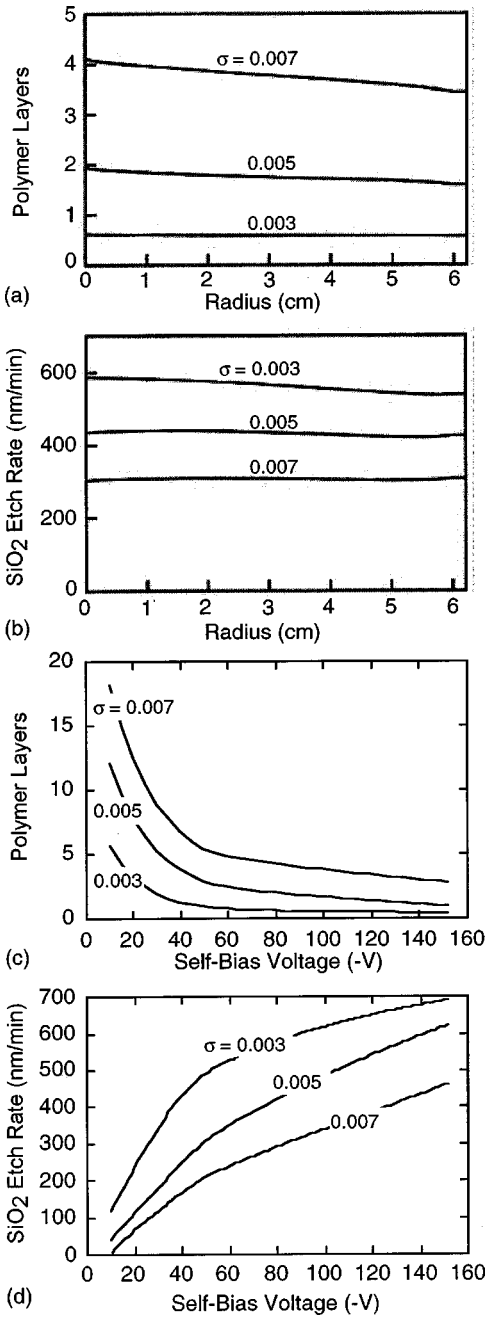

FIG. 9. Surface process properties as a function of neutral sticking coefficient. (a) SiO_2 etch rate, and (b) polymer thickness, as a function of radius, for different sticking coefficients. (c) SiO_2 etch rate, and (d) polymer thickness, as a function of self-bias voltage, for different sticking coefficients.

rate increases noticeably with increasing p_0 for $V_s > 100$ V biases, as shown in Fig. 10(b). For the 170 V bias, the polymer thickness drops below one monolayer at large p_0, and so the etch rate tends to saturate with increasing p_0.

Direct reactions of ions and the wafer surface may occur in SiO_2 etching when the polymer thickness is small or site coverage is spotty. We investigated the sensitivity of the model to the probability of direct ion etching of SiF_3 surface species that produces volatile SiF_4 and exposes new SiO_2. This reaction is $C_xF^+_{y\,g} + SiF_{3s} \rightarrow C_xF_{y-1} + SiF_{4g} + SiO_{2s}$. In the base case, we assumed an ion etch probability, η, of 0.11

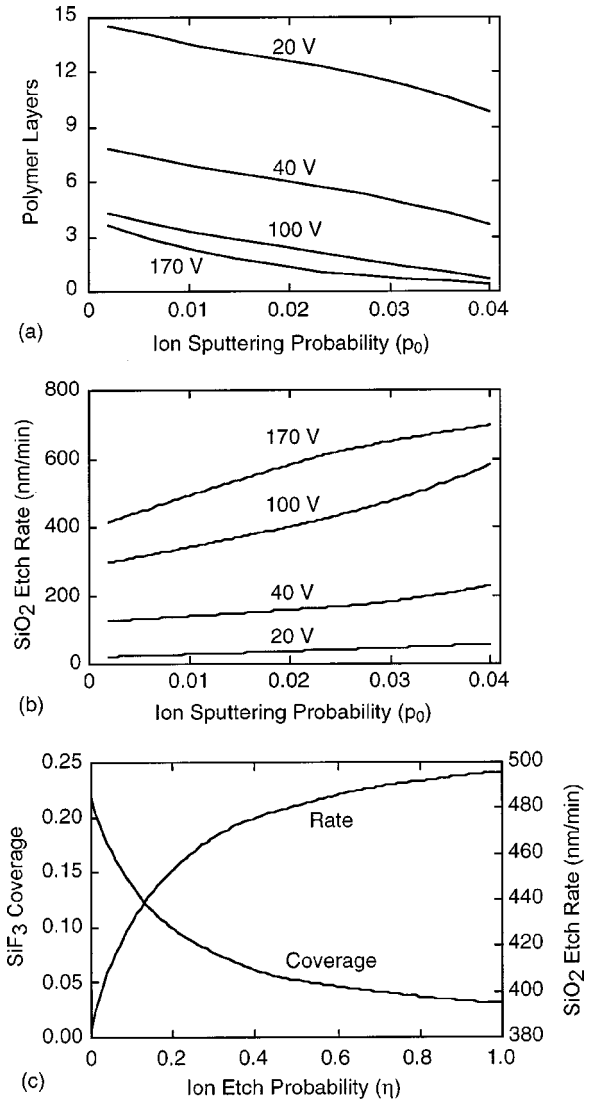

FIG. 10. Surface process properties as a function of ion sputtering and etch probability (p_0) for different substrate biases. (a) Polymer thickness. (b) SiO_2 etch rate. (c) SiF_3 coverage and SiO_2 etch rate.

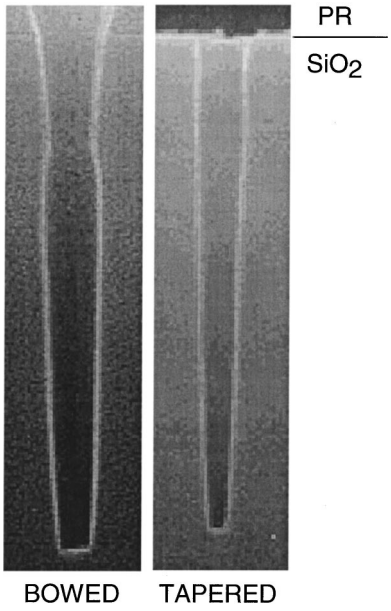

FIG. 11. Examples of bowed and tapered etch profiles in fluorocarbon etching of SiO_2. (PR denotes photoresist.)

for a 70 eV ion hitting a bare surface (no polymer coverage). According to Eqs. (3) and (5), this corresponds to an effective etch probability of 0.064, as the base case has an average ion energy of 98 eV and a polymer coverage of 1.94 layers. The SiO_2 etch rate and the SiF_3 surface coverage as a function of η are shown in Fig. 10(c). With increasing η from 0 to 1, a decrease of SiF_3 coverage from 0.22 to 0.03 is obtained, which is accompanied by an increase of the etch rate from 380 to 495 nm/min. When η is small (<0.4), the SiF_3 coverage drops rapidly with increasing η, and the etch rate increases as removal of SiF_3 is a rate limiting step. When η is large (>0.4) and the SiF_3 coverage is small, further increasing η does not significantly change the coverage as the desorption is no longer rate limiting. As a result, the etch rate changes little with increasing η.

We note that the selectivities discussed here may be low in comparison with state-of-the-art oxide etching processes used for microelectronics fabrication in industry. We have chosen operating conditions and gas mixtures for which experimental data are available for validation and calibration, and which result in lower selectivities. We expect that the surface reaction mechanism proposed here will extend to the more complex gas mixtures used in industry to obtain higher selectivities.

V. PROFILE SIMULATIONS OF SiO_2 ETCHING BY C_2F_6 PLASMA

In microelectronics fabrication, one frequent and challenging application of fluorocarbon plasma etching of SiO_2 is to produce vias with high aspect ratio (HAR). Due to complex surface reactions on the bottom and sidewalls of the trench, etch profiles often deviate from the ideal which are vertically straight. For example, SiO_2 profiles for similar process conditions are shown in Fig. 11. Process conditions with low bias and high polymerizing fluxes tend to produce tapered profiles. High bias and low polymerizing fluxes produce bowed profiles. To investigate the mechanisms responsible for SiO_2 profile evolution, we used the surface reaction mechanism described above in the MCFPM. Since the MCFPM uses a Monte Carlo algorithm for surface reactions, the analytical approach describing the polymer thickness dependent reactions which was used in the equipment scale model had to be modified. In the feature scale model, thick polymer coverage occurs by ''stacking'' mesh cells representing the polymer on the surface. The height of the polymer mesh cells is equivalent to polymer thickness. The polymer thickness dependent plasma–wafer reactions are realized by the fact that increasing thickness of polymer cells decreases the probability for the wafer surface to be exposed to the plasma and react. We note that mask erosion can have a significant effect on profile evolution. We are limiting this study to the details of the oxide etch mechanism. Although

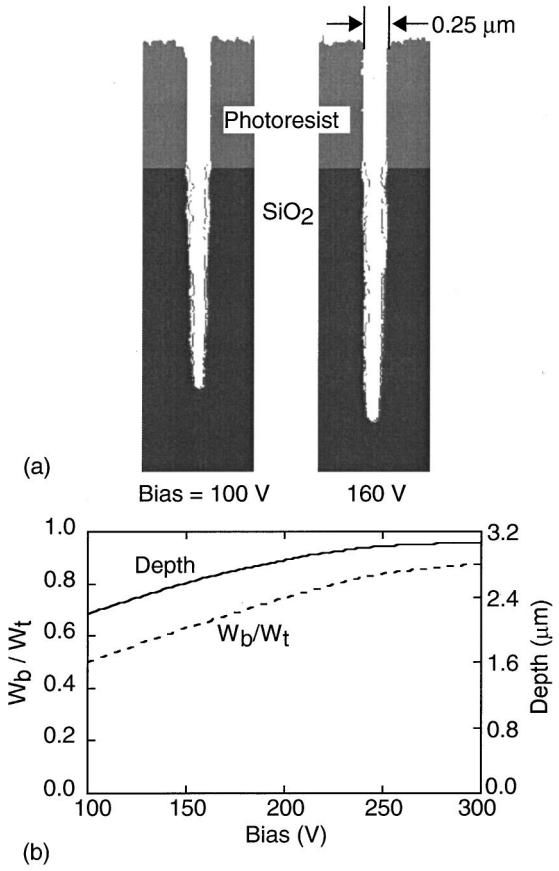

FIG. 12. Influence of substrate bias on features. (a) High aspect ratio profiles of SiO_2 etched by a C_2F_6 plasma at 100 and 160 V biases. The profiles taper near the bottom. (b) W_b/W_t and trench depth as a function of substrate bias. W_b refers to the trench width 0.5 μm above the trench bottom, and W_t is the trench width at the top. Results were obtained after equal etch times. Increasing bias improves profile control and increases etch rate.

some mask erosion by direct sputtering was allowed, the mask remains largely intact and so its etching does not significantly affect the profiles.

It has been found experimentally that in HAR etching of SiO_2 by fluorocarbon plasmas, tapering of the trench generally occurs under conditions where there is excessive passivation.[25] We simulated HAR SiO_2 etching by the previously described C_2F_6 plasma. Trench profiles after equal etch times at 100 and 160 V substrate biases are shown in Fig. 12(a). There is a shrinking of the feature width at the bottom of the trench for both biases. The trench is less tapered and deeper with the higher bias after equal etch times. The tapered profiles are attributed to the strong sidewall passivation. Since neutral fluxes have broad incident angular distributions and low sticking coefficients, they reflect many times in the trench, eventually sticking to the sidewalls and the bottom of the trench at nearly equal rates. However, ion bombardment has a narrow ion angular distribution. As a result, most ions at best graze the sidewalls and reflect specularly with a low reaction probability,[26] while the bottom of the trench receives a larger normal flux having higher reaction probabilities. The grazing ion bombardment of the sidewalls is inefficient at removing polymers, leading to stronger sidewall passivation as compared to that at the bottom. During etching the sidewall passivation grows, shadowing the area of the bottom of the trench that can receive vertical ion bombardment, leading to a tapered profile of the trench. With increasing bias voltage, the incident ion energy increases, resulting in a larger sputtering yield of the polymer. The increasing polymer consumption leads to both a broader critical dimension at the bottom and a higher etch rate, as shown in Fig. 12(a).

To investigate the dependence of critical dimension on bias, we performed profile simulations for a range of higher biases. We use the ratio of the trench width 0.5 μm above the bottom of the trench (W_b) to the width at the top (W_t) to quantify the degree of tapering, and the trench depth after equal etch times to quantify the etch rate. W_b/W_t and the trench depth as a function of the substrate bias are shown in Fig. 12(b). With increasing substrate bias from 100 to 300 V, both W_b/W_t and the trench depth rapidly increase due to the increasing sputtering of the passivation and higher ion activation rates. In the high bias regime, both metrics tend to saturate because insufficient passivation limits the etching process. The dependence of the etch rate on the substrate bias obtained from our profile simulation agrees well with that obtained from the equipment scale modeling discussed earlier.

As tapering is produced by sidewall passivation, its magnitude is related to the ratio of the flux of passivating neutrals to ions, $\beta = \Phi_n/\Phi_{\text{ion}}$. To investigate the influence of β on the etch profiles, we artificially scaled the neutral fluxes from the base case (β=12) while keeping other parameters the same. (Although the fluxes so obtained may not specifically correspond to given process parameters, this methodology is helpful in understanding the mechanism of etching.) Trench profiles for different β are shown in Fig. 13(a). W_b/W_t and trench depth after equal etch times as a function of β are shown in Fig. 13(b). The base case produces a tapered profile due to the strong passivation. With decreasing β, the sidewall passivation decreases, leading to increasing etch rates and a less tapered profiles. A nearly straight trench was obtained with β=8.4. A further decrease of β, however, leads to insufficient sidewall passivation. As a result, the sidewalls are also etched to some degree, leading to a bowed profile at β=6, as shown in Fig. 13(a). The ratio of critical dimensions, W_b/W_t, then exceeds unity. These results indicate that controlling β is important to controlling the shape of HAR features.

One effective approach for controlling β is to dilute the C_2F_6 with a chemically inert gas. By adding Ar to the feedstock C_2F_6, the passivating neutral densities are decreased, while ion densities are to some degree enhanced due to the larger ionization cross sections of Ar and Penning processes. The end result is a decrease in β. To investigate the effect of this gas mixture on HAR feature profiles, we performed simulations at different Ar/C_2F_6 ratios while keeping other process parameters the same as in the base case. The profiles after reaching nearly equal depths are shown in Fig. 14(a). β and W_b/W_t as a function of Ar fraction are shown in Fig.

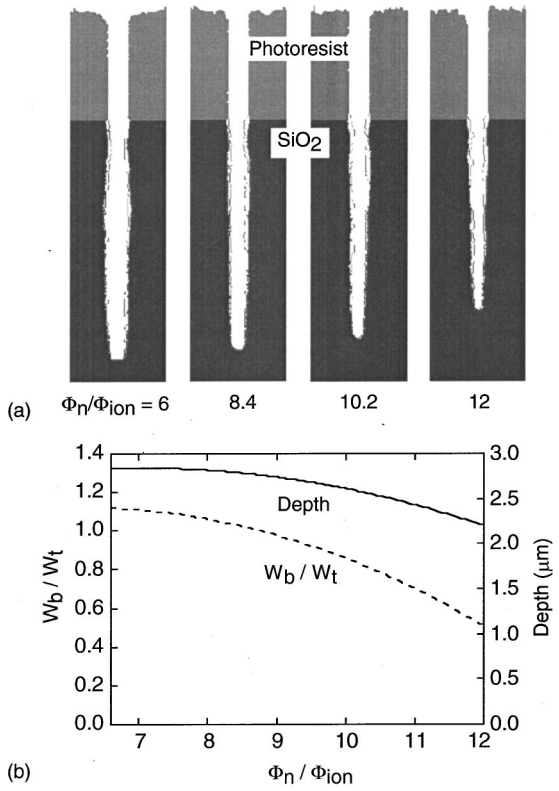

FIG. 13. Influence of passivating neutral to ion flux ratio (Φ_n/Φ_{ion}) on SiO_2 features. (a) Profiles for different Φ_n/Φ_{ion} ratios. (b) W_b/W_t and trench depth as a function of Φ_n/Φ_{ion}. Results were obtained after equal etch times. Decreasing Φ_n/Φ_{ion} increases etch rate and W_b/W_t, with low values producing bowing.

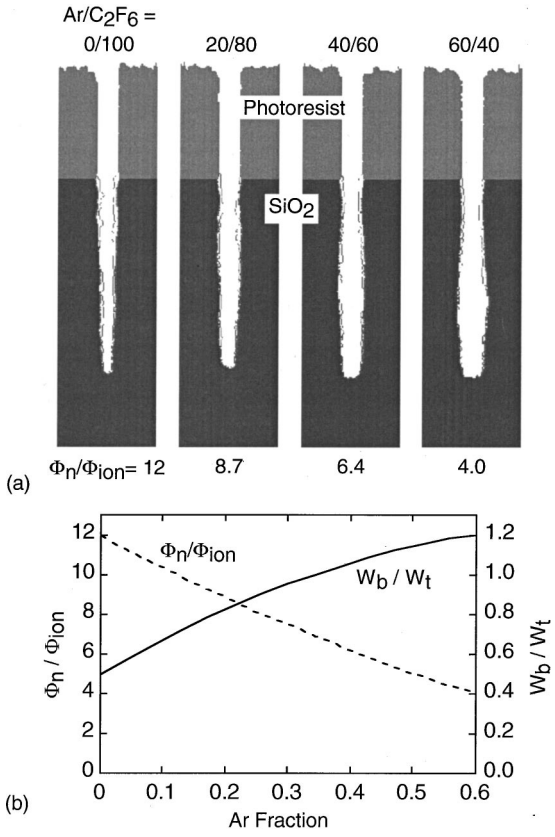

FIG. 14. Influence of Ar fraction in an Ar/C_2F_6 ICP on SiO_2 features. (a) Profiles for different Ar/C_2F_6 ratios. (b) Passivating neutral to ion flux ratio (Φ_n/Φ_{ion}), and W_b/W_t, as a function of Ar fraction in the gas source. Increasing the Ar fraction decreases Φ_n/Φ_{ion}, thereby increasing W_b/W_t.

14(b). β decreases by a factor of 3 by increasing the Ar fraction to 60%. The base case, which has no Ar, produced a tapered profile. With 20% Ar and a decrease in β to 8.7, a nearly straight trench was obtained. Further increase of the Ar fraction to 40% leads to a bowed profile with $W_b/W_t > 1$ due to there being insufficient sidewall protection by passivation. The bowing further increases with an increase in the Ar fraction to 60%.

Although the purpose of the study was to investigate SiO_2 etch mechanisms, it is appropriate to briefly comment on the consequences of Si/SiO_2 selectivity in profile control. For example, profiles were simulated for low bias conditions with pure C_2F_6 where the selectivity of SiO_2/Si was large. The resulting profiles near an underlying Si layer are shown in Fig. 15(a). The etch depth and W_b/W_t as a function of time are shown in Fig. 15(b). For these plots, the polymer has been removed prior to plotting to show only the Si, SiO_2, and plasma interfaces. For highly polymerizing conditions and low bias, an etch stop often occurs at the SiO_2/Si interface. The etch stop consists of a layer, sometimes growing to a plug, of polymer on the Si which dramatically slows or terminates etching at the interface.[25] We see this behavior in Fig. 15 where the etch feature and etch depth ''bottom out'' at the SiO_2/Si interface. For these conditions, a low rate of etching of Si continues, providing a SiO_2/Si selectivity of $\approx 28-30$. Note that there is also a small degree of aspect

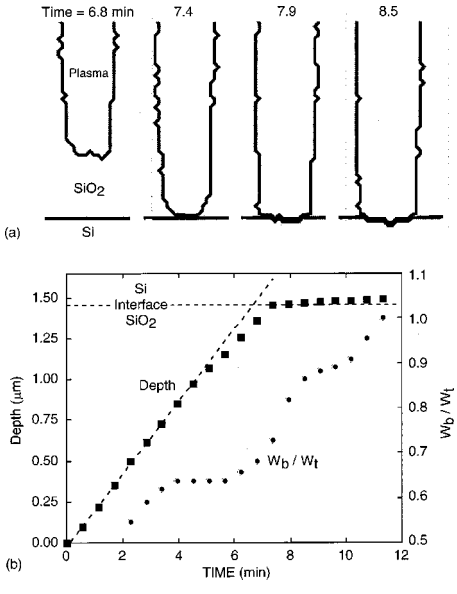

FIG. 15. Feature properties for etching SiO_2 down to a Si underlayer. (a) Etch profiles near the interface where polymer and surface complexes have been removed from the plots. (b) Etch depth and W_b/W_t as a function of time. A 50% overetch enables a tapered feature at the interface to broaden, producing $W_b/W_t = 1.0$. Note a small degree of aspect ratio dependent etch rate as the etch rate slows with etch depth.

ratio dependent etching where the etch rate slows as the trench deepens. The etch stop at the SiO_2/Si interface enables a tapered profile ($W_b/W_t<1$) to recover to become a straight profile ($W_b/W_t\approx1$). The overetch time, in this case $\approx$50%, combined with high selectivity, allows the corners of the trench to be etched, thereby straightening the sidewalls. Further overetching will result in a bowed profile.

VI. CONCLUDING REMARKS

A surface reaction mechanism accounting for polymer passivation and passivation thickness dependent rates has been developed for SiO_2 and Si etching by fluorocarbon plasmas. The polymer is formed by C_xF_y neutral deposition, and is consumed by ion sputtering, F atom etching and SiO_2 etching. Low-energy ion activation of surface sites assists neutral polymerization. SiO_2 etching is preceded by neutral passivation, and it evolves through either ion chemical sputtering or successive fluorination. The passivation is provided in large part by the interface layer of the polymer. Since plasma–wafer interactions involve a transfer of energy and species through the polymer, their rates scale inversely with the polymer thickness. The etch selectivity of SiO_2 over Si is attributed to the thinner polymer passivation on the SiO_2 as a result of polymer consuming reactions at the wafer surface.

The reaction mechanism was first applied to an integrated plasma–surface model to investigate SiO_2 etching by an ICP sustained in C_2F_6. Increasing substrate bias increases the ion bombarding energy while hardly changing other plasma properties. Consequently, the polymer thickness decreases with increasing bias due to increasing polymer yield by ion sputtering, producing an increase in the etch rate. Increasing E_c, the maximum ion activation energy for polymerization, leads to increasing polymer thickness and lower etch rate in the low bias region. Good agreement with experiments for the bias dependent etch rates of SiO_2 and Si was obtained for $E_c=65$ eV. The SiO_2 etch rate saturates at high ion energy due to the depletion of passivation. Therefore increasing neutral fluxes at high biases increases the etch rate while decreasing the etch rate at low bias where etching is not limited by the availability of passivation.

The surface reaction mechanism was also applied to a feature scale model to investigate the SiO_2 profiles produced by the C_2F_6 discharge. Simulations produced tapered trenches for HAR SiO_2 etching, an effect attributed to the strong sidewall passivation. Increasing bias leads to less tapered profiles due to increasing ion sputtering of the polymer. The dependence of the etch rate on the substrate bias obtained in the feature model (the increase of etch rate until saturating at high biases) is similar to that obtained in the equipment scale model. A tapered profile transitions to a straight profile and further to a bowed feature with decreasing passivating neutral to ion flux ratio (Φ_n/Φ_{ion}), accompanied by an increase in the etch rate. Φ_n/Φ_{ion} decreases with increasing Ar fraction in an Ar/C_2F_6 mixture, and profile optimization can be achieved by controlling the Ar fraction.

One of the differences between *a priori* simulation and modeling of the type discussed here is that in modeling, the lack of absolute knowledge of fundamental processes or coefficients, or exorbitant complexity in the real mechanism, requires some degree of either simplification, heuriticism, or judgement in developing the model. Weakness in the model described here is that, due to the complexity of the phenomena being addressed and the unlikelihood that all required coefficients and parameters will be known with precision, simplification, heuriticism, and judgement were all brought into play. A reviewer asked how tentative this model is and if there are alternatives. The mechanisms we have proposed do not uniquely explain the experiments and the coefficients we have derived are likely not unique within that framework. We encourage the reviewer and the reader to view this model and those of other workers as frameworks with which one can develop and test hypothesis to explain, reproduce, and explain complex, physical phenomena. We expect that with the additional insight afforded by this model, that the mechanism can be refined by other workers within the general framework proposed here.

ACKNOWLEDGMENTS

This work was supported by the Semiconductor Research Corporation, Applied Materials, DARPA/AFOSR, and the National Science Foundation (CTS99-74962). The authors thank Dr. Chunshi Cui for her insights into oxide etching reaction mechanisms and for providing scanning electron micrographs.

[1]N. R. Rueger, M. F. Doemling, M. Schaepkens, J. J. Beulens, T. E. F. M. Standaert, and G. S. Oehrlein, J. Vac. Sci. Technol. A **17**, 2492 (1999).
[2]A. J. Bariya, C. W. Frank, and J. P. McVittie, J. Electrochem. Soc. **137**, 2575 (1990).
[3]B. E. E. Kastenmerier, P. J. Matsuo, G. S. Oehrlein, and J. G. Langan, J. Vac. Sci. Technol. A **16**, 2047 (1998).
[4]S. Samukawa and S. Furuoya, Jpn. J. Appl. Phys., Part 2 **32**, L1289 (1993).
[5]M. Schaepkens, R. C. M. Bosch, T. E. F. M. Standaert, and G. S. Oehrlein, J. Vac. Sci. Technol. A **16**, 2099 (1998).
[6]T. E. F. M. Standaert, M. Schaepkens, N. R. Rueger, P. G. M. Sebel, G. S. Oehlein, and J. M. Cook, J. Vac. Sci. Technol. A **16**, 239 (1998).
[7]K. Miyata, M. Hori, and T. Goto, J. Vac. Sci. Technol. A **14**, 2083 (1996).
[8]M. Kitamura, H. Akiya, and T. Urisu, J. Vac. Sci. Technol. B **7**, 14 (1989).
[9]M. Schaepkens, T. E. F. M. Standaert, N. R. Rueger, P. G. M. Sebel, G. S. Oehlein, and J. M. Cook, J. Vac. Sci. Technol. A **17**, 26 (1999).
[10]N. R. Rueger, J. J. Beulens, M. Schaepkens, M. F. Doemling, J. M. Mirza, T. E. F. M. Standaert, and G. S. Oehrlein, J. Vac. Sci. Technol. A **15**, 1881 (1997).
[11]C. F. Abrams and D. B. Graves, J. Appl. Phys. **86**, 5938 (1999).
[12]D. Zhang and M. J. Kushner, J. Appl. Phys. **87**, 1060 (2000).
[13]R. J. Hoekstra and M. J. Kushner, J. Vac. Sci. Technol. B **16**, 2102 (1998).
[14]R. J. Hoekstra, M. J. Grapperhaus, and M. J. Kushner, J. Vac. Sci. Technol. A **15**, 1913 (1997).
[15]K. Teii, M. Hori, and T. Goto, J. Appl. Phys. **87**, 7185 (2000).
[16]J. P. Booth, G. Cunge, P. Chabert, and N. Sadeghi, J. Appl. Phys. **85**, 3097 (1999).

[17]M. Inayoshi, M. Ito, M. Hori, and T. Goto, J. Vac. Sci. Technol. A **16**, 233 (1998).
[18]D. C. Gray, I. Tepermeister, and H. H. Sawin, Proceedings of the Second International Conference on Reactive Plasmas, Yokohama, Japan, 19–21 January 1994.
[19]G. S. Oehrlein and J. F. Rembetski, IBM J. Res. Dev. **36**, 140 (1992).
[20]P. J. Mastuo, B. E. E. Kastenmeier, J. J. Beulens, and G. S. Oehrlein, J. Vac. Sci. Technol. A **15**, 1801 (1997).
[21]C. F. Abrams and D. B. Graves, J. Vac. Sci. Technol. A **18**, 411 (2000).
[22]M. Schaepkens, G. S. Oehlein, and J. M. Cook, J. Vac. Sci. Technol. B **18**, 848 (2000).
[23]T. Tatsumi, M. Matsui, M. Okigawa, and M. Sekine, J. Vac. Sci. Technol. B **18**, 1897 (2000).
[24]J. W. Butterbaugh, D. C. Gray, and H. H. Sawin, J. Vac. Sci. Technol. B **9**, 1461 (1991).
[25]A. C. Westerheim, A. H. Labun, J. H. Dubash, J. C. Arnold, H. H. Sawin, and V. Yu-Wang, J. Vac. Sci. Technol. A **13**, 853 (1995).
[26]B. A. Helmer and D. B. Graves, J. Vac. Sci. Technol. A **16**, 3502 (1998).